Journal of Membrane Science 563 (2018) 726–733

Contents lists available at ScienceDirect

Journal of Membrane Science

journal homepage: www.elsevier.com/locate/memsci

Molecular design of double crosslinked sulfonated polyphenylsulfone /polybenzimidazole blend membranes for an efficient hydrogen purification

Ali Naderi[a], Akbar Asadi Tashvigh[a], Tai-Shung Chung[a,*], Martin Weber[b], Christian Maletzko[c]

[a] Department of Chemical and Biomolecular Engineering, National University of Singapore, Singapore 117585, Singapore
[b] Advanced Materials and Systems Research, BASF SE, RAP/OUB - B1, 67056 Ludwigshafen, Germany
[c] Performance Materials, BASF SE, G-PMF/SU-F206, 67056 Ludwigshafen, Germany

ARTICLE INFO

Keywords:
Homogeneous blend
Double crosslinking
Gas separation
Fractional free volume (FFV)
Hydrogen purification
CO_2 capture

ABSTRACT

This study, for the first time, demonstrates a new double-crosslinking approach to manipulate the microstructure and gas separation performance of PBI membranes for H_2/CO_2 separation at 150 °C. The PBI membranes were firstly blended with sulfonated polyphenylsulfone (sPPSU) as an ionic-crosslinker and then α,α′-dibromo-p-xylene (DBX) as a covalent crosslinker with the aid of thermal annealing. Experiments show that PBI and sPPSU interact on the molecular level. Different from conventional blends, the PBI/sPPSU blend membranes show both enhanced chemical resistance and greater fractional free volume (FFV) after annealing at elevated temperatures because of chain motion and ionic crosslinking. As a result, the blend membranes maintain their high permeability after annealing. The DBX addition further improves the chemical resistance and tightens the inter-chain spacing that results in membranes with a small FFV and pore size. Consequently, the DBX cross-linked blend membranes retain their high gas pair selectivity at high temperatures. The 50/50 PBI/sPPSU blend membrane crosslinked by 0.7 wt% DBX at 300 °C possesses the best separation performance surpassing the Robeson's upper bound. It has an impressively H_2 permeability of 46.2 Barrer and a high H_2/CO_2 selectivity of 9.9 at 150 °C.

1. Introduction

Hydrogen production is under high demands in industries for oil refining, ammonia production and fuel cells. Currently, steam reforming of hydrocarbons followed by the water–gas shift reaction is a predominant technology for hydrogen production. In this process, the produced hydrogen is mainly mixed with CO_2, H_2O and others [1–4]. Commercially available hydrogen separation processes are amine absorption, cryogenic distillation and pressure swing adsorption (PSA) which are energy intensive. Comparing with these technologies, membrane separation technology has many advantages such as small footprint, high energy efficiency, cost competitiveness, easy scale-up and environmental friendliness [5]. However, the achievable H_2 purity of the latter is much lower than that of the former [2].

To overcome this drawback, several approaches have been adopted to modify polymeric membranes with enhanced H_2/CO_2 separation performance such as design of novel polymers with a tight d-space [6,7], doping [8–10], polymer blends [10–13] and crosslinking of polyimides [14–18]. Generally, diamino crosslinking modifications of polyimides resulted in a higher selectivity with the expense of permeability, while membranes derived from polybenzimidazole (PBI) had a reasonable selectivity but a low permeability. As a result, mixed matrix membranes (MMMs) consisting of (1) polyimides and metal-organic frameworks (MOFs) [19,20], (2) PBI and MOFs [21–23] and (3) PBI/palladium [24], and membranes made from (1) PBI/stainless steel [25], (2) cross-linked PBI [26] and (3) doped PBI [9] were proposed in the last decade for efficient H_2/CO_2 separation. Generally, the incorporation of MOFs significantly enlarged the permeability, while the crosslinking modifications tightened the chain structure and enhanced the selectivity.

Concurrently, other carbon and inorganic materials discovered in the last decade such as graphene oxide [GO] and MOFs were also extensively studied for H_2/CO_2 separation in order to take advantages of their high molecular-sieving ability [27–34]. For example, two-dimensional (2D) layered materials such as graphene and graphene oxide (GO) were stacked with aligned subnanometer channels to form selective membranes for H_2 separation [31,32], while MOF nano-sheets were fabricated with a distinctive aperture between the kinetic diameters of H_2 and CO_2 [27–29,33,34]. However, at this present, it is still difficult to fabricate large pieces of membranes made from GO and MOFs without defects for hydrogen purification.

Since the size-sieving ability of PBI-based membranes for H_2/CO_2

* Correspondence author.
E-mail address: chencts@nus.edu.sg (T.-S. Chung).

https://doi.org/10.1016/j.memsci.2018.06.033
Received 2 May 2018; Received in revised form 1 June 2018; Accepted 16 June 2018
Available online 22 June 2018
0376-7388/

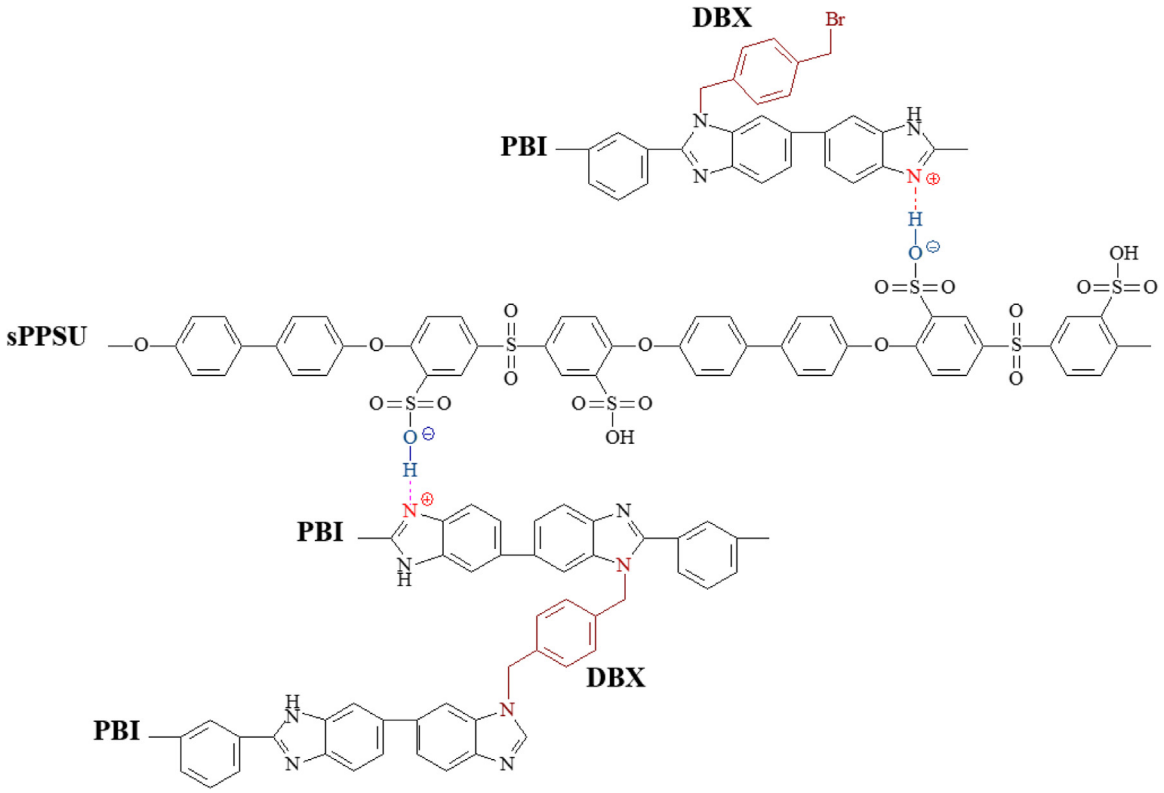

Fig. 1. Schematic diagram of the possible ionic and covalent crosslinking interactions in the membranes.

separation could be remarkably enhanced by (1) ionic interactions between PBI and polyprotic acids [9] and (2) chemical cross-linking reaction with the aid of terephthaloyl chloride (TCL) [26], Prof. Lin's works inspired us to explore the feasibility of manipulating the size-sieving properties of blend membranes made from PBI and sulfonated polyphenylsulfone (sPPSU) with the aid of α,α′-dibromo-p-xylene (DBX). sPPSU is chosen because it has good chemical and thermal properties [35]. In addition, it has strong ionic interactions with PBI on the molecular level [36], while DBX is chosen as the crosslinker because it would covalently crosslink with PBI [37]. Fig. 1 illustrates the possible ionic and covalent crosslinking reactions between PBI and sPPSU as well as PBI and DBX. Thus, they may form two possible networks in the microstructure of blend membranes so that one may be able to manipulate their gas transport properties for H_2/CO_2 separation. Therefore, X-ray photoelectron spectroscopy (XPS) and Fourier transform infrared spectroscopy (FTIR) would be employed in the first part of this study to investigate the existence of ionic and covalent chemical structures. Afterwards, the gas transport properties of the ionic and chemical crosslinked membranes for H_2/CO_2 separation would be examined. In addition, their mixed gas properties at 150 °C would be conducted to explore the applicability of these membranes for hydrogen purification under industrial conditions at high temperatures.

2. Experimental

2.1. Material

Sulfonated polyphenylsulfone (sPPSU) with a sulfonation degree of 2.5 mol% was synthesized by BASF SE, Germany via direct copolymerization by using the monomer of 4,4′-dichlorodiphenyl sulfone (DCDPS) [35,36]. A Celazoles S26 polybenzimidazole (PBI, MW = 27000 $gmol^{-1}$) solution with the composition of 72.5 wt% dimethylacetamide(DMAc), 26 wt% PBI and 1.5 wt% LiCl was provided by PBI Performance Products Inc. (USA). α,α′-Dibromo-p- xylene (DBX, 97%) purchased from Sigma Aldrich was utilized as the crosslinking agent. DMAc (HPLC grade) was supplied by Merck and used as solvent for the two polymers.

2.2. Fabrication of membranes

The dense flat membranes of PBI/sPPSU blends were prepared by a solution casting method. Five solutions containing 2 wt% of the two polymers and their three blends at weight ratios of 25/75, 50/50 and 75/25 were prepared using DMAc as a solvent. For instance, a 3.6 g blend polymer was dissolved in 180 g DMAc and the solution was stirred overnight. In addition, two more 50/50 wt% PBI/sPPSU solutions containing the DBX crosslinker at 0.3 wt% and 0.7 wt% were prepared to study the effect of covalent crosslinking in the presence of ionic crosslinking on gas separation performance. The solutions were filtered by a 1 μm polytetrafluoroethylene (PTFE) filter and cast in petri dishes. Thereafter, the solvent of the solutions was gradually evaporated by placing the petri dishes in a vacuum oven for 24 h at 50 °C. The oven temperature was increased with a heating rate of 1 °C/min to 150 °C and held there for 12 h to remove the residual solvent, followed by naturally cooling to ambient temperature. The membrane thickness was around 80 ± 5 μm measured by a Digimatic indicator (IDC-112B-5).

Table 1 tabulates the compositions of all membranes. Each membrane was labeled according to its PBI and DBX percentages. For example, 75PBI means that the blend membrane contains 75/25 PBI/sPPSU in weight ratio. The membranes cast from pure polymers were indicated by their own names (i.e., sPPSU and PBI), while membranes consisting of DBX were attached by yDBX where y is the weight percentage of the crosslinker in the solution. In addition, the temperature of any additional thermal treatment would be attached at the end of their names (e.g. the 50PBI-0.3DBX-300 membrane was thermally treated at 300 °C). The thermal treatment was performed using a VBF-1200X-H8 vacuum furnace (MTI Corp, USA) with a heating rate of 5 °C/min under vacuum from room temperature to a pre-determined temperature (i.e., 300 °C or 400 °C) and held there for 120 min. Thereafter,

Table 1
Compositions of the dope solutions.

Membrane	sPPSU/PBI[a]	DMAc (wt%)	DBX(wt%)
PBI	0/100	98	–
75PBI	25/75	98	–
50PBI	50/50	98	–
25PBI	75/25	98	–
sPPSU	100/25	98	–
50PBI-0.3DBX	50/50	97.7	0.3
50PBI-0.7DBX	50/50	97.3	0.7

[a] Total polymer concentration = 2 wt%.

the membrane was cooled down naturally to room temperature under vacuum. All flat sheet membranes were flexible and mechanically strong for permeation tests. Fig. 2a and b show the appearance of the manufactured membranes and their micrographs observed under a polar light microscope (PLM), respectively. As shown in Fig. 2, all blend membranes are transparent, suggesting their good homogeneity.

2.3. Characterizations

The surface morphology of the fabricated membranes was investigated by using an Olympus BX50 PLM with the aid of Image Pro Plus 3.0 software. The chemical bondings of the DBX crosslinked and non-DBX crosslinked membranes were studied using Fourier transform infrared spectroscopy (FTIR- VERTEX 70/70 v) with a fixed angle ATR mode in the range of 400–4000 cm^{-1}. X-ray photoelectron spectroscopy (XPS, Kratos AXIS UltraDLD, Kratos Analytical Ltd., England) was employed to analyze the ionic crosslinking reaction between PBI and sPPSU. The analyses were conducted using a monochromatic X-ray of 15 kV and 100 W to investigate the binding energy level of N1s on the membrane surface.

To validate the occurrence of the ionic and covalent crosslinking of the fabricated membranes and their effects on the robustness of membranes, three pieces of each membrane sample were immersed in DMAc (a good solvent for both PBI and sPPSU) and the amount of undissolved solid was measured as a function of time. The fabricated membranes with fixed masses (m_0) were immersed in DMAc to extract their insoluble portions at 35 °C for a specific duration (i.e., 6 h, 12 h, 24 h and 48 h). Thereafter the remaining insoluble membranes were dried under vacuum at 150 °C for 12 h and then weighted to measure their masses (m_1). The percentage of undissolved solid was calculated by using Eq. (1) as follows:

$$Undissolved\ solid\ \ \% = \frac{m_1}{m_0} \times 100 \tag{1}$$

Fractional free volume (FFV) was evaluated using Positron annihilation lifetime spectroscopy (PALS). The fabricated membranes were stacked on both sides of a ^{22}Na positron source. The tests were performed by imposing the positron beam with a counting rate of around 200 counts per second. The spectrum of each membrane was collected after reaching two million counts. The quantitative information of the pore size and free volume content is ascribed to the pick-off annihilation of the ortho-positronium (*o-Ps*) which is the triplet bound state of a positron and an electron. There is a correlation between the annihilation lifetime of o-*Ps* (τ_3 in nano-second) and the mean free volume radius R (Å) according to the semi-empirical model for spherical cavity as follows [38,39]:

$$\tau_3 = \frac{1}{2}\left[1 - \frac{R}{R+\Delta R} + \frac{1}{2\pi}\sin\left(\frac{2\pi R}{R+\Delta R}\right)\right]^{-1} \tag{2}$$

where ΔR refer to an empirical parameter (1.66 Å). The PATFIT-88 program was employed to analyze the obtained PALS data assuming a Gaussian distribution of the fitted lifetime components. The relative FFV was calculated according to the Williams–Landel–Ferry (WFL) equation as follows [40,41]:

$$FFV = 0.0018 I_3 \langle \nu_f(\tau_3) \rangle = 0.0018 I_3 \left(\frac{4}{3}\pi R^3\right) \tag{3}$$

where I_3 refer to the ortho-positronium intensity (%) for the estimated pick-off lifetime (τ_3). ν_f is the mean free volume ($Å^3$) of a cavity in the polymer matrix. R indicates the mean free-volume radius (Å).

2.4. Gas transport properties

The pure gas permeability of the membranes was conducted on a variable-pressure constant-volume gas permeation cell [42]. The fabricated membranes were located in the permeation cell and vacuumed for 12 h at 35 °C before tests. The permeability of gases was measured in the sequence of H_2 and CO_2, and each data point was repeated for three times with the average deviation of less than 5%. The coefficient of gas permeability was measured considering the increment of the downstream pressure rate (dP/dt) according to the Eq. (4):

$$P = \frac{237 \times 10^{10}}{760} \frac{Vl}{AT\left(P_2 \times \frac{76}{14.7}\right)} \left(\frac{dp}{dt}\right) \tag{4}$$

where P is the gas permeability in Barrer (1 Barrer = 1×10^{-10} cm^3 (STP).cm cm^{-2} s^{-1} cm Hg^{-1}), V refers to the volume of the downstream chamber (cm^3), A is the effective membrane area (cm^2), l denotes the membrane thickness (cm), T symbolizes the operating temperature (K) and p_2 is defined as the upstream pressure of the permeation cell (psi). The ideal selectivity between H_2 and CO_2 gases through the membranes was calculated with aid of Eq. (5):

$$\alpha_{H_2/CO_2} = \frac{P_{H_2}}{P_{CO_2}} \tag{5}$$

where P_{H2} and P_{CO2} represent the gas permeability of H_2 and CO_2 gases, respectively.

The mixed gas permeation properties of the fabricated membranes were investigated using a binary 50% H_2 and 50% CO_2 gas mixture. The membranes were tested at 7 atm and 150 °C. The permeability of H_2 and CO_2 were calculated according to Eq. (6) and Eq. (7) as follows:

$$P_{H_2} = \frac{273 \times 10^{10}}{760} \frac{y_{H_2} \times V \times l}{AT\left(P_2 \times \phi_{H_2} \times x_{H_2} \times \frac{76}{14.7}\right)} \frac{dp}{dt} \tag{6}$$

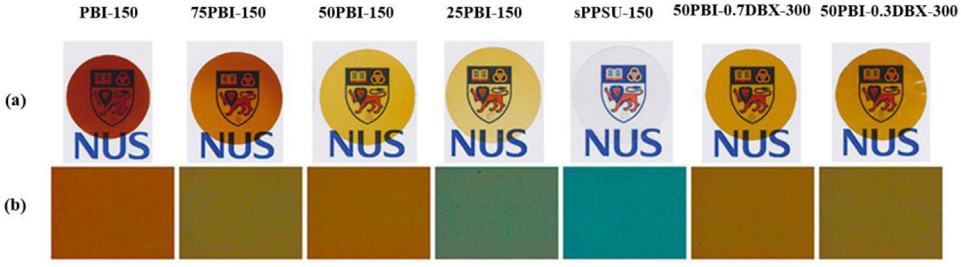

Fig. 2. The appearance of membranes, (a) their photographs and (b) their PLM micrographs.

$$P_{CO_2} = \frac{273 \times 10^{10}}{760} \frac{y_{CO_2} \times V \times l}{AT\left(P_2 \times \phi_{CO_2} \times x_{CO_2} \times \frac{76}{14.7}\right)} \quad (7)$$

where x and y denote the mole fractions of gases in the feed and permeate, respectively. ϕ_{H_2} and ϕ_{CO_2} designate the fugacity coefficients of the upstream for H_2 and CO_2, respectively. The rest symbols have the same meanings as explained in Eq. (4) and Eq. (5). The mixed gas selectivity of H_2 over CO_2 was calculated according to Eq. (5).

2.5. Measurements of gas sorption

The CO_2 sorption of the membranes was examined by using a XEMISseries static sorption microbalance [43]. Prior to the assessment, each membrane with a weight of 90–110 mg was loaded into the sample chamber and vacuumed for 18 h. The CO_2 sorption isotherm was conducted with a ramped pressure from 50 mbar to 10 bar. To measure the sorption at elevated temperatures, a water bath was used to keep the temperatures of both the reference and sample at 35 °C, while a system's standard furnace was applied for testing the sorption at 150 °C. The CO_2 solubility coefficient (cm^3 (STP) cm^{-3} (membranes) atm^{-1}) of the membranes was calculated using Eq. (8) as follows:

$$S = \frac{C}{P} \quad (8)$$

where C is the total concentration of the adsorbed CO_2 in the membrane (cm^3(STP) cm^{-3}). The CO_2 diffusion coefficient of the membranes could be subsequently calculated according to Eq. (9):

$$D = \frac{P}{S} \quad (9)$$

3. Results and discussion

3.1. Ionic and covalent cross-linking reactions

The occurrence of covalent and ionic crosslinking reactions in the membranes was confirmed by FTIR and XPS, respectively. Fig. 3 shows the FTIR spectra of the non-DBX-crosslinked and DBX-crosslinked membranes. The appearance of the characteristic peak at 3420 cm^{-1} is ascribed to non-hydrogen bonded N–H stretching of PBI. Besides, the O-H stretching peak may exist and overlap with the free N-H stretching peak. Two characteristic peaks at 2920 cm^{-1} and 2850 cm^{-1} which appear for the DBX-crosslinked membranes can be assigned to C-H stretching (the terminal C in DBX) and C-N stretching (the link between DBX and PBI), respectively, as illustrated in Fig. 1 [37,44]. These peaks confirm the occurrence of the crosslinking reaction between PBI and DBX.

Fig. 4 displays the XPS spectra of surface chemistry on 50PBI-150, 50PBI-300 and 50PBI-400 membranes. The N(1s) spectra of the

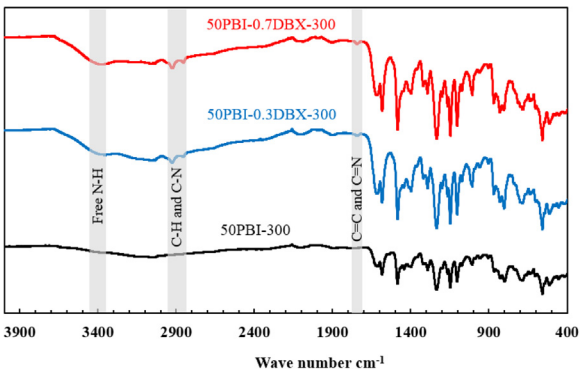

Fig. 3. FT-IR spectra of uncrosslinked and DBX crosslinked 50PBI-300 membranes.

membranes represent three peaks which can be ascribed to PBI and its ionic interaction with sPPSU. The peaks at ~398.2 and ~ 400.1 eV can be attributed to imine (=N-) and amine (-NH-) groups of the imidazole rings in PBI, respectively. The peak at ~ 401.2 eV represents the protonated imine ($-NH^+=$), indicating the existence of the ionic interaction between PBI and sPPSU [45,46]. As illustrated in Fig. 4a, b and c, the peak area of the protonated imine is increasing while the peak areas of both imine and amine are decreasing with an increase in thermal treatment temperature. This can be due to the enhanced ionic interaction between sPPSU and PBI with the aid of thermal treatment. In other words, the polymer chains at high temperatures have sufficient energy to perform segmental motions and rearrangement so that the sulfonic acid groups of sPPSU can meet the imine groups of PBI easier; hence the ionic crosslinking reaction occurs more effectively.

Table 2 displays the effects of ionic and covalent crosslinking modifications on robustness of the membranes. The 50PBI-150 membrane is immediately dissolved in DMAc after a few minutes. However, the 50PBI-300 membrane is fully dissolved in the solvent after 12 h. This phenomenon confirms the higher degree of ionic crosslinking in the 50PBI-300 membrane when increasing the thermal treatment temperature to 300 °C, as proved by XPS results (Fig. 4). On the other hand, membranes containing DBX display a good solvent resistance properties, indicating that the covalent crosslinking reaction has occurred in these membranes, as proved by FTIR spectra (Fig. 3). Clearly, the occurrence of both ionic and covalent interactions in the fabricated membranes significantly enhances their chemical resistance.

3.2. Gas separation characteristics of the blend membranes

Table 3 shows the gas permeability and ideal selectivity of PBI/sPPSU blends, and DBX crosslinked PBI/sPPSU blends thermally treated at different temperatures. Comparing the first five membranes heat treated at the same temperature of 150 °C, the PBI-150 membrane has the highest H_2/CO_2 selectivity of 6.7 and the lowest H_2 permeability of 2.9 Barrer, while the sPPSU-150 membrane displays the lowest H_2/CO_2 selectivity of 1.8 and the highest H_2 permeability of 14.64 Barrer. In addition, their blend membranes show gas separation properties in terms of permeability and selectivity apparently proportional to their dominant component. Since the blend membranes show good homogeneity as observed by PLM in Fig. 2, the rule of semi-logarithmic addition is employed to fit their gas transport properties as follows [47,48]:

$$\ln P_b = \phi_1 \ln P_1 + \phi_2 \ln P_2 \quad (10)$$

$$\ln\left(\frac{P_1}{P_2}\right) = \phi_1 \ln\left(\frac{P_1}{P_2}\right)_1 + \phi_2 ln\left(\frac{P_1}{P_2}\right)_2 \quad (11)$$

where P_b is the permeability of the polymer blend, P_1 and P_2 are the permeability of components 1 and 2, ϕ_1 and ϕ_2 are the volume fractions of components 1 and 2, respectively.

Fig. 5a and b compare the experimental and predicted permeability and selectivity of these five membranes. Interestingly, they match quite well possibly due to the high miscibility of these two polymers and the formation of ionic interaction between them. Since the 50PBI-150 membrane possesses a lower CO_2 permeability and a higher H_2/CO_2 selectivity compared to the predicted data, it is selected for further studies.

3.3. The effects of thermal treatment temperature on gas separation performance

Table 3 also shows the gas transport properties of 50PBI membranes as a function of thermal treatment temperature. A comparison of samples 3, 6 and 7 indicates that the H_2/CO_2 selectivity increases from 4.6 to 6 as the thermal treatment temperature increases from 150 °C to 300 °C, and then decreases to 4.6 again if the treatment temperature

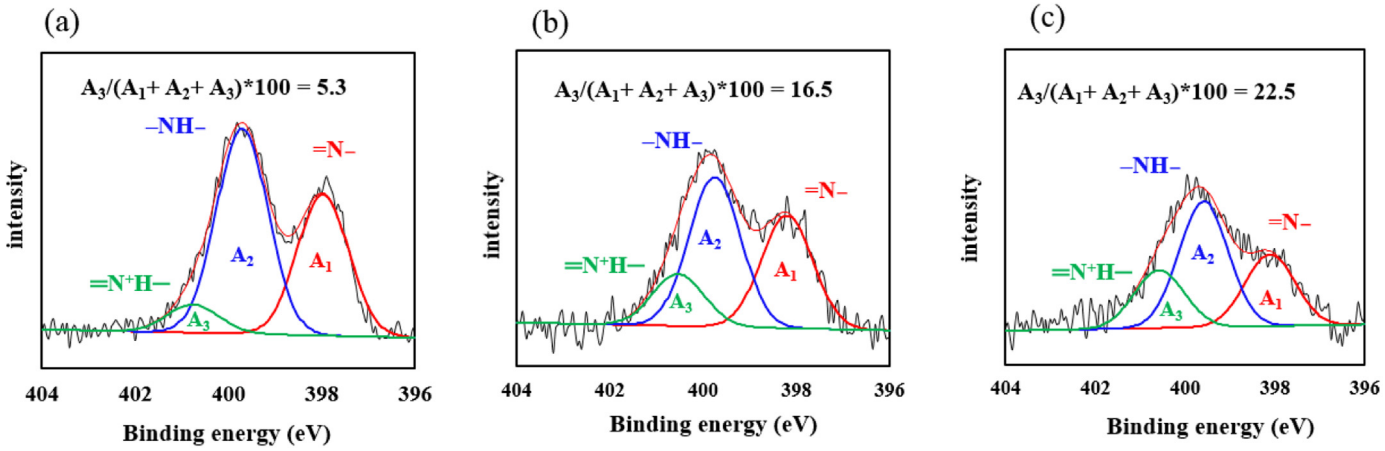

Fig. 4. XPS N 1 s narrow scan on the top surfaces of 50PBI membranes thermally treated at (a) 150 °C, (b) 300 °C and (c) 400 °C.

Table 2
Undissolved solid percentage of the membranes as a function of time.

Membranes	Undissolved solid (%) after 6 h in DMAc	Undissolved solid (%) after 12 h in DMAc	Undissolved solid (%) after 24 h in DMAc	Undissolved solid (%) after 48 h in DMAc
50PBI-150	0	0	0	0
50PBI-300	58	20	0	0
50PBI-0.3DBX-300	100	100	100	99
50PBI-0.7DBX-300	100	100	100	99

Table 3
Gas separation performance of the membranes at 3.5 atm and 35 °C.

No	Membrane code	Permeability (Barrer)[a]		Ideal selectivity
		H_2	CO_2	H_2/CO_2
1	PBI-150	2.90	0.43	6.7
2	75PBI-150	3.74	0.79	4.8
3	50PBI-150	5.82	1.26	4.6
4	25PBI-150	9.18	3.17	2.9
5	sPPSU-150	14.64	8.13	1.8
6	50PBI-300	6.24	1.03	6.1
7	50PBI-400	6.48	1.42	4.6
8	50PBI-0.3DBX-300	5.45	0.99	5.5
9	50PBI-0.7DBX-300	4.42	0.68	6.5

[a] 1 Barrer = 1×10^{-10} cm^3 (STP)cm cm^{-2} s^{-1} cm Hg^{-1}. The data were measured at 3.5 atm and 35 °C.

further increases to 400 °C. Since the selectivity of a membrane for a gas pair is the ratio of their permeability coefficients and the permeability is a product of diffusivity coefficient (D) and solubility coefficient (S) based on the solution-diffusion model, FFV, d-space and CO_2 sorption of the membranes are therefore measured in order to elucidate the complicated relationship among them.

Table 4 tabulates the FFV values of 50PBI membranes calculated from the orthopositronium lifetime (T_3) intensity (I_3) and means free volume radius (R_3). They follow the order of 50PBI-150 < 50PBI-300 < 50PBI-400, indicating that FFV increases with an increase in thermal treatment temperature. This interesting phenomenon may arise from the fact that a higher thermal treatment temperature results in a higher degree of ionic crosslinking interaction. In other words, as proved in Fig. 4, the polymer chains have greater segmental motions at a higher temperature, this facilitates the ionic crosslinking reaction between the sulfonic acid groups of sPPSU and the imine groups of PBI. Since sPPSU is a macromolecule, the chain movement also causes an inefficient packing in the blend membranes. Consequently, the 50PBI-400 membrane has the highest FFV. The XRD data shown in Fig. 6 and Table 5 are consistent with the PALS results. On the other hand, introducing the DBX crosslinker into the blend membranes leads to a decrement in d-spacing from 4.69 A° to 4.45 A° because the formation of covalent bonds between DBX and PBI so that the chain-chain distance is shortened.

The CO_2 sorption is determined based on the gravimetric method, while the H_2 sorption is not measured due to its extremely low sorption in polymers [49]. Fig. 7a and b display the CO_2 sorption and solubility coefficients of the membranes as a function of pressure, respectively. The diffusivity coefficients of the membranes are calculated using the solubility coefficients at 3.5 atm from Fig. 7b and tabulated in Table 6. Consistent with the order of FFV values, the diffusivity coefficients of the thermal-treated 50PBI membranes follows the sequence of 50PBI-150 < 50PBI-300 < 50PBI-400. However, the 50PBI-300 membrane has the lowest solubility of 3.39 cm^3(STP)/cm^3(polymer) atm among these three membranes. It is known that gas sorption in a nonporous polymeric membrane is associated with its interactions with the polymer and the FFV value of the membrane [42]. Although 50PBI-300 has a FFV higher than 50-PBI-150, its low CO_2 sorption implies that the former has a lower polymer-CO_2 interaction than the latter. According to Torrisi et al. study, CO_2 can be adsorbed by the formation of hydrogen bonds between the oxygen of CO_2 and the hydrogen of SO_3H [50]. Therefore, the lowest CO_2 sorption of the 50PBI-300 membrane may be caused by the fact that its SO_3H groups have been fully involved in the ionic interaction with PBI and cannot contribute to the CO_2 adsorption via hydrogen bonding. This lowest CO_2 sorption also makes the 50PBI-300 membrane to have the highest H_2/CO_2 selectivity among these three membranes, as shown in samples 3, 6 and 7 of Table 3. Therefore, 300 °C is selected as the optimal temperature for the thermal treatment of 50PBI membranes in this study.

3.4. The effect of covalent crosslinking on gas separation performance

Stoichiometrically 1.71 g DBX is required to fully crosslink 1 g PBI. Therefore, 0.3 g and 0.7 g DBX per gram of PBI were added into the blend solutions to obtain the percentages of crosslinking at around 20%

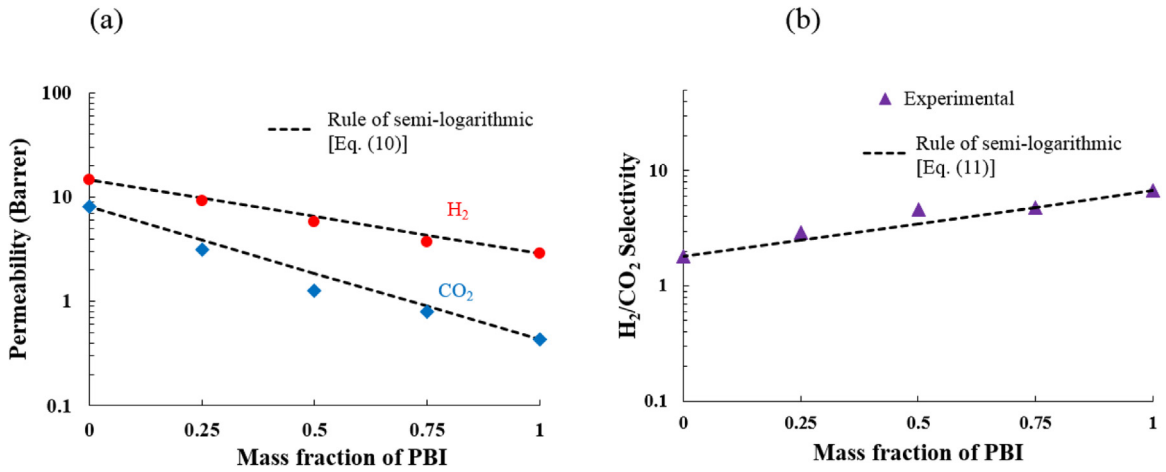

Fig. 5. Comparison between experimental and predicted data for (a) permeability of H_2 and CO_2 (b) H_2/CO_2 selectivity.

Table 4
PALS data of the membranes.

Membranes	τ_3 (ns)	I_3 (%)	R_3 (Å)	FFV (%)
50PBI-150	1.61	14.72	2.46	1.66
50PBI-300	1.62	15.35	2.48	1.76
50PBI-400	1.75	16.31	2.62	2.21
50PBI-0.3DBX-300	1.57	5.50	2.43	0.59
50PBI-0.7DBX-300	1.39	4.52	2.22	0.37

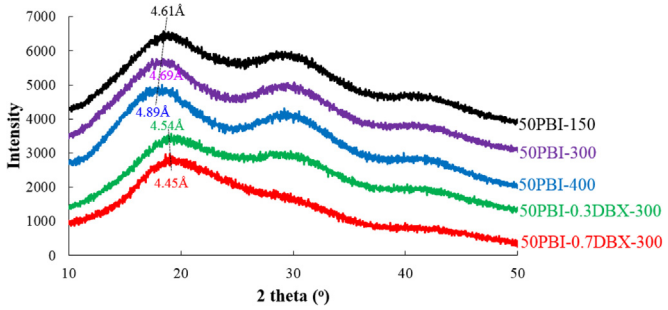

Fig. 6. XRD spectra of the membranes.

Table 5
XRD data of the membranes.

Membranes	2 theta (deg.)	*d*-spacing (Å)	*FFV* (%)
50PBI-150	19.25	4.61	1.66
50PBI-300	18.86	4.69	1.76
50PBI-400	18.12	4.89	2.21
50PBI-0.3DBX-300	19.52	4.54	0.59
50PBI-0.7DBX-300	19.91	4.45	0.37

and 40%, respectively (i.e., resulting in partially covalent-crosslinked membranes). Consequently, there are many N sites in PBI chains which can be concurrently ionically crosslinked by sPPSU as well. A comparison of samples 6, 8 and 9 in Table 3 shows that the H_2/CO_2 selectivity decreases from 6.1 to 5.5 and then increases to 6.5 as the percentage of crosslinking (i.e., the DBX amount) increases, while their permeability declines monotonically with the amount of DBX addition.

The decreases in H_2 and CO_2 permeability can be easily understood because DBX induces the covalent crosslinking reaction with PBI that tightens the intersegmental polymer chains, reduces FFV and pore size, as proved by XRD and PALS results (Fig. 6, Table 4 and Table 5). As a result, the CO_2 diffusivity of these membranes decreases as the DBX amount in the blend membranes increases. Since both permeability and diffusivity decrease with increasing DBX content, the gas transport properties of these membranes are dominated by the diffusivity coefficient.

On the other hand, the CO_2 solubility of the membranes interestingly increases in the order of 50PBI-0.7DBX-300 > 50PBI-0.3DBX-300 > 50PBI-300 although their FFV values decreases as the DBX content increases. This strange phenomenon may arise from the fact that the available SO_3H sites which are not ionically crosslinked increases when the DBX content is increased. In other words, the addition of DBX reduces the number of free N sites in PBI to crosslink ionically with SO_3H groups. Therefore, the 50PBI-0.7DBX-300 membrane has more free SO_3H sites to adsorb CO_2 than 50PBI-0.3DBX-300 and 50PBI-300.

3.5. Mixed gas measurements

Since the gas leaving the water-gas-shift reaction mainly contains H_2 (56%) and CO_2 (40%) at 150 °C or above [3], it is essential to investigate the performance of the current membranes at similar conditions. Therefore, the 50PBI-300, 50PBI-0.3DBX-300 and 50PBI-0.7DBX-300 membranes were investigated using a binary gas mixture of 50/50H_2/CO_2 at 150 °C with a feed pressure of 7 atm. Fig. 8 shows the results and compares them with the literature and Robeson upper bound. The 50PBI-0.7DBX-300 membrane has a H_2 permeability of 46.2 Barrer and a H_2/CO_2 selectivity of 9.9 that is significantly above the 2008 upper bound, indicating its outstanding H_2/CO_2 separation performance at 150 °C. However, the separation performance of the other two membranes are only at or approaching to the upper bound.

Fig. 9 shows the CO_2 sorption of 50PBI-300 and 50PBI-0.7DBX-300 at 150 °C and compares them with their CO_2 sorption at 35 °C. Obviously, the amount of CO_2 sorption decreases by increasing the temperature because it is harder to condense CO_2 at a higher temperature. Nevertheless, the 50PBI-0.7DBX-300 membrane has a higher adsorbed CO_2 concentration than the 50PBI-300 membrane at both operating temperatures because the former has more available SO_3H groups than the latter as discussed in Section 3.3. Table 7 summarizes the permeability, solubility and diffusivity coefficients of these two membranes at 150 °C. The 50PBI-0.7DBX-300 membrane has a remarkably lower diffusivity coefficient than the 50PBI-300 membrane (316.7 vs. 714.6×10^{-10} cm^2 s^{-1}). This can be due to the more efficient chain packing and subsequently lower FFV of the DBX-crosslinked membrane than that of the non-DBX-crosslinked membrane. As a result, 50PBI-0.7DBX-300 shows a 10% lower CO_2 permeability than 50PBI-300.

Because the 50PBI-0.7DBX-300 membrane has a higher H_2 permeability and a lower CO_2 permeability than the 50PBI-300 membrane (Fig. 8 and Table 7), it leads to have superior H_2/CO_2 gas separation

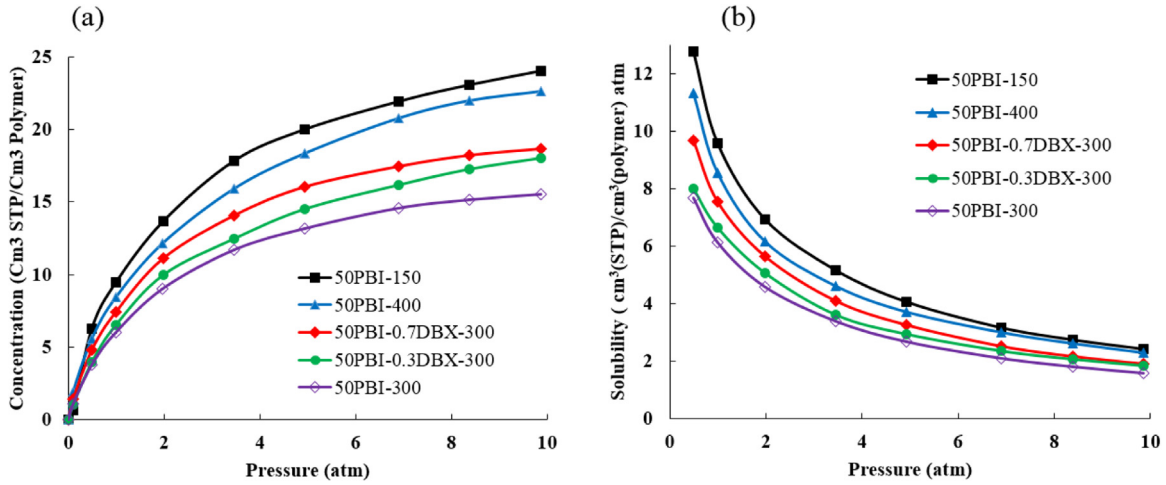

Fig. 7. (a) CO_2 sorption isotherms at 35 °C and (b) solubility coefficient as a function of pressure for the membranes.

Table 6
Pure gas permeation properties of 50PBI membranes at 3.5 bar and 35 °C.

Membranes	Permeability[a] CO_2	Solubility CO_2	Diffusivity[b] CO_2	FFV (%)
50PBI-150	1.26	5.16	18.55	1.66
50PBI-300	1.03	3.39	23.09	1.76
50PBI-400	1.42	4.61	28.98	2.21
50PBI-0.3DBX-300[c]	0.99	3.60	20.89	0.59
50PBI-0.7DBX-300	0.68	4.08	12.66	0.37

[a] 1 Barrer = 1×10^{-10} cm^3 (STP)cm cm^{-2} s^{-1} cm Hg^{-1}.
[b] Solubility (cm^3(STP)/cm^3(polymer) atm. The data were measured at 3.5 atm and 35 °C.
[c] Diffusivity = 1×10^{-10} cm^2 s^{-1}.

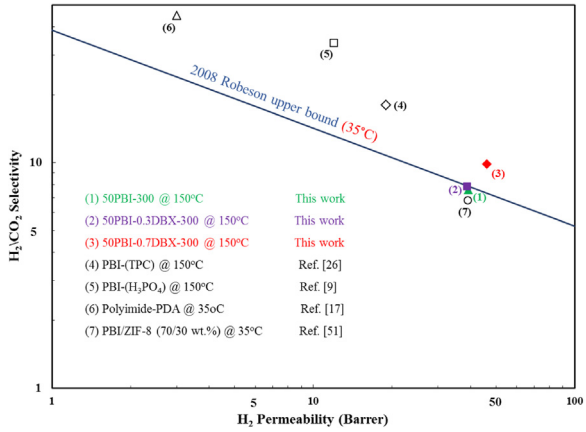

Fig. 8. Mixed gas performance of the membranes for H_2/CO_2 separation [26], [9], [17], [51].

performance at 150 °C. When comparing it with other state-of-the-art membranes such as mixed matrix membranes (MMMs) containing MOFs, crosslinked PBI membranes with various crosslinkers and other polymeric membranes at 150 °C, as illustrated in Fig. 8, the newly developed membrane has unique H_2/CO_2 separation performance with an impressive H_2 permeability of 46.2 Barrer. Since this in-situ double-crosslinked blend membrane can be easily manufactured and scaled up, the in-situ double crosslinking method may open up new strategies to tailor make polymeric membranes with enhanced gas separation performance.

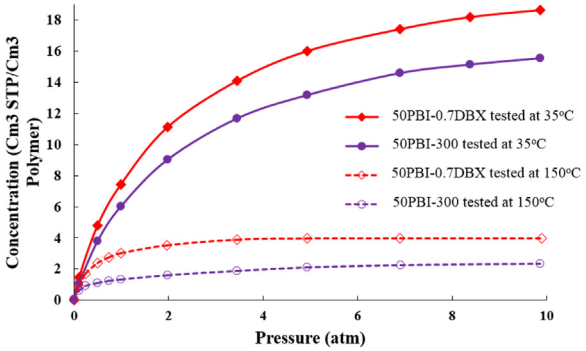

Fig. 9. CO_2 sorption isotherms of 50PBI-300 and 50PBI-0.7DBX-300 membranes at 35 °C and 150 °C.

Table 7
CO_2 permeability, diffusivity and solubility coefficients at 3.5 bar and 150 °C.

Membranes	Permeability[a] CO_2	Solubility CO_2	Diffusivity[b] CO_2
50PBI-300	5.2	0.55	714.5
50PBI-0.7DBX-300[c]	4.7	1.13	316.7

[a] 1 Barrer = 1×10^{-10} cm^3 (STP)cm cm^{-2} s^{-1} cm Hg^{-1}.
[b] Solubility (cm^3(STP)/cm^3(polymer) atm. The data were measured at 3.5 atm and 150 °C.
[c] Diffusivity = 1×10^{-10} cm^2 s^{-1}.

4. Conclusion

We have proved, for the first time, a double crosslinking technique to enhance the H_2/CO_2 selectivity of PBI/sPPSU blends with the aid of DBX crosslinker for hydrogen purification at high temperatures. It is found that PBI and sPPSU interact on the molecular level via ionically crosslinking. Interestingly, the PBI/sPPSU blend membranes not only show enhanced chemical resistance but also possess greater FFV after being thermally treated at 300 °C because of chain motion and ionic crosslinking. As a result, the blend membranes maintain their high permeability after annealing. The addition of DBX further improves the chemical resistance and tightens the inter-chain spacing that results in blend membranes with a small FFV and pore size. Consequently, the DBX cross-linked blend membranes retain their high gas pair selectivity at high temperatures. The 50PBI-0.7DBX-300 membrane possesses the best separation performance with a H_2 permeability of 46.2 and a H_2/CO_2 selectivity of 9.9 at 150 °C. Comparing to the other membranes in

the literature, this membrane has separation performance above the Robeson's upper bound and has an impressive high H_2 permeability.

Acknowledgments

This research is supported by BASF SE, Germany for the project "The Evaluation and Characterization of Polyarylethers for Membrane Applications" (grant number R-279-000-411-597), National University of Singapore, Dean's Office of Faculty of Engineering for the project entitled "Natural Gas Centre" (grant number R-261-508-001-646) and Department of Chemical and Biomolecular Engineering for the project "Membrane Research for CO_2 Capture" (grant number R-279-000-505-133). A. Naderi would like to extend his gratitude to Dr. Youchang Xiao for his useful discussion and help.

Appendix A. Supporting information

Supplementary data associated with this article can be found in the online version at http://dx.doi.org/10.1016/j.memsci.2018.06.033.

References

[1] H. Lin, E. Van Wagner, B.D. Freeman, L.G. Toy, R.P. Gupta, Plasticization-enhanced hydrogen purification using polymeric membranes, Science 311 (2006) 639–642.
[2] L. Shao, B.T. Low, T.S. Chung, A.R. Greenberg, Polymeric membranes for the hydrogen economy: contemporary approaches and prospects for the future, J. Membr. Sci. 327 (2009) 18–31.
[3] H. Lin, Integrated membrane material and process development for gas separation, Curr. Opin. Chem. Eng. 4 (2014) 54–61.
[4] T.C. Merkel, M. Zhou, R.W. Baker, Carbon dioxide capture with membranes at an IGCC power plant, J. Membr. Sci. 389 (2012) 441–450.
[5] X. Jiang, S. Li, L. Shao, Pushing CO2-philic membrane performance to the limit by designing semi-interpenetrating networks (SIPN) for sustainable CO 2 separations, Energy Environ. Sci. 10 (2017) 1339–1344.
[6] Z. Wang, T. Chen, J. Xu, Gas transport properties of novel cardo poly (aryl ether ketone) s with pendant alkyl groups, Macromolecules 33 (2000) 5672–5679.
[7] C. Camacho-Zuniga, F. Ruiz-Trevino, M. Zolotukhin, L. Del Castillo, J. Guzman, J. Chavez, G. Torres, N. Gileva, E. Sedova, Gas transport properties of new aromatic cardo poly (aryl ether ketone) s, J. Membr. Sci. 283 (2006) 393–398.
[8] M.R. Anderson, B.R. Mattes, H. Reiss, R.B. Kaner, Conjugated polymer films for gas separations, Science 252 (1991) 1412–1415.
[9] L. Zhu, M.T. Swihart, H. Lin, Unprecedented size-sieving ability in polybenzimidazole doped with polyprotic acids for membrane H_2/CO_2 separation, Energy Environ. Sci. (2018).
[10] N.K. Acharya, V. Kulshrestha, K. Awasthi, A.K. Jain, M. Singh, Y.K. Vijay, Hydrogen separation in doped and blend polymer membranes, Int. J. Hydrog. Energy 33 (2008) 327–331.
[11] M.E. Rezac, B. Schoberl, Transport and thermal properties of poly (ether imide)/acetylene-terminated monomer blends, J. Membr. Sci. 156 (1999) 211–222.
[12] T.M. Su, I.J. Ball, J.A. Conklin, S.C. Huang, R.K. Larson, S.L. Nguyen, Polyaniline/polyimide blends for pervaporation and gas separation studies, Synth. Met. 84 (1997) 801–802.
[13] S.S. Hosseini, M.M. Teoh, T.S. Chung, Hydrogen separation and purification in membranes of miscible polymer blends with interpenetration networks, Polymer 49 (2008) 1594–1603.
[14] R.A. Hayes, Amine-modified polyimide membranes, US Patent No. 4,981,497, 1991.
[15] L. Shao, T.S. Chung, S.H. Goh, K.P. Pramoda, Transport properties of cross-linked polyimide membranes induced by different generations of diaminobutane (DAB) dendrimers, J. Membr. Sci. 238 (2004) 153–163.
[16] L. Shao, L. Liu, S.-X. Cheng, Y.-D. Huang, J. Ma, Comparison of diamino cross-linking in different polyimide solutions and membranes by precipitation observation and gas transport, J. Membr. Sci. 312 (2008) 174–185.
[17] B.T. Low, Y. Xiao, T.S. Chung, Y. Liu, Simultaneous occurrence of chemical grafting, crosslinking and etching on the surface of polyimide membranes and their impact on H_2/CO_2 separation, Macromolecules 41 (2008) 1297–1309.
[18] C.M. Aberg, A.E. Ozcam, J.M. Majikes, M.A. Seyam, R.J. Spontak, Extended chemical crosslinking of a thermoplastic polyimide: macroscopic and microscopic property development, Macromol. Rapid Commun. 29 (2008) 1461–1466.
[19] S. Japip, K.S. Liao, T.S. Chung, Molecularly tuned free volume of vapor cross-linked 6FDA-durene/ZIF-71 MMMs for H2/CO_2 separation at 150° C, Adv. Mater. 29 (2017).
[20] Z. Wang, D. Wang, S. Zhang, L. Hu, J. Jin, Interfacial design of mixed matrix membranes for improved gas separation performance, Adv. Mater. 28 (2016) 3399–3405.
[21] T.X. Yang, Y.C. Xiao, T.S. Chung, Poly-/metal-benzimidazole nano-composite membranes for hydrogen purification, Energy Environ. Sci. 4 (2011) 4171–4180.
[22] T.X. Yang, G.M. Shi, T.S. Chung, Symmetric and asymmetric zeolitic imidazolate frameworks (ZIFs)/polybenzimidazole (PBI) nanocomposite membranes for hydrogen purification at high temperatures, Adv. Energy Mater. 2 (2012) 1358–1367.
[23] T.X. Yang, T.S. Chung, Room-temperature synthesis of ZIF-90 nanocrystals and the derived nano-composite membranes for hydrogen separation, J. Mater. Chem. A 1 (2013) 6081–6090.
[24] L.F. Villalobos, R. Hilke, F.H. Akhtar, K.V. Peinemann, Fabrication of polybenzimidazole/palladium nanoparticles hollow fiber membranes for hydrogen purification, Adv. Energy Mater. 8 (2018).
[25] K.A. Berchtold, R.P. Singh, J.S. Young, K.W. Dudeck, Polybenzimidazole composite membranes for high temperature synthesis gas separations, J. Membr. Sci. 415 (2012) 265–270.
[26] L. Zhu, M.T. Swihart, H. Lin, Tightening polybenzimidazole (PBI) nanostructure via chemical cross-linking for membrane H_2/CO_2 separation, J. Mater. Chem. A 5 (2017) 19914–19923.
[27] Y. Peng, Y. Li, Y. Ban, H. Jin, W. Jiao, X. Liu, W. Yang, Metal-organic framework nanosheets as building blocks for molecular sieving membranes, Science 346 (2014) 1356–1359.
[28] W. Yang, Y. Peng, Y. Li, Y. Ban, Two-dimensional metal-organic framework nanosheets for membrane-based gas separation, Angew. Chem. Int. Ed. (2017).
[29] C. Kong, H. Du, L. Chen, B. Chen, Nanoscale MOF/organosilica membranes on tubular ceramic substrates for highly selective gas separation, Energy Environ. Sci. 10 (2017) 1812–1819.
[30] M. Yu, H.H. Funke, R.D. Noble, J.L. Falconer, H_2 separation using defect-free, inorganic composite membranes, J. Am. Chem. Soc. 133 (2011) 1748–1750.
[31] H. Li, Z. Song, X. Zhang, Y. Huang, S. Li, Y. Mao, H.J. Ploehn, Y. Bao, M. Yu, Ultrathin, molecular-sieving graphene oxide membranes for selective hydrogen separation, Science 342 (2013) 95–98.
[32] H.W. Kim, H.W. Yoon, S.-M. Yoon, B.M. Yoo, B.K. Ahn, Y.H. Cho, H.J. Shin, H. Yang, U. Paik, S. Kwon, Selective gas transport through few-layered graphene and graphene oxide membranes, Science 342 (2013) 91–95.
[33] Y.S. Li, F.Y. Liang, H. Bux, A. Feldhoff, W.S. Yang, J. Caro, Molecular sieve membrane: supported metal–organic framework with high hydrogen selectivity, Angew. Chem. Int. Ed. 122 (2010) 558–561.
[34] Z. Kang, M. Xue, L. Fan, L. Huang, L. Guo, G. Wei, B. Chen, S. Qiu, Highly selective sieving of small gas molecules by using an ultra-microporous metal–organic framework membrane, Energy Environ. Sci. 7 (2014) 4053–4060.
[35] Y.N. Feng, M. Weber, C. Maletzko, T.S. Chung, Facile fabrication of sulfonated polyphenylenesulfone (sPPSU) membranes with high separation performances for organic solvent nanofiltration, Membr. Sci. 549 (2018) 550–558.
[36] A.A. Tashvigh, L. Luo, T.S. Chung, M. Weber, C. Maletzko, A novel ionically crosslinked sulfonated polyphenylsulfone (sPPSU) membrane for organic solvent nanofiltration (OSN), J. Membr. Sci. 545 (2018) 221–228.
[37] A.A. Tashvigh, L. Luo, T.S. Chung, M. Weber, C. Maletzko, Performance enhancement in organic solvent nanofiltration by double crosslinking technique using sulfonated polyphenylsulfone (sPPSU) and polybenzimidazole (PBI), J. Membr. Sci. 551 (2018) 204–213.
[38] Y. Jean, J.D. Van Horn, W.-S. Hung, K.-R. Lee, Perspective of positron annihilation spectroscopy in polymers, Macromolecules 46 (2013) 7133–7145.
[39] H. Chen, W.-S. Hung, C.-H. Lo, S.-H. Huang, M.-L. Cheng, G. Liu, K.-R. Lee, J.-Y. Lai, Y.-M. Sun, C.-C. Hu, Free-volume depth profile of polymeric membranes studied by positron annihilation spectroscopy: layer structure from interfacial polymerization, Macromolecules 40 (2007) 7542–7557.
[40] Y. Jean, P. Mallon, D. Schrader, Principles and Applications of Positron and Positronium Chemistry, World Scientific, 2003.
[41] Y. Jean, Positron Annihilation Spectroscopy for Chemical Analysis: A Novel Probe for Microstructural Analysis of Polymers, Microchem. J 42 (1990), pp. 72–102.
[42] P. Li, T.S. Chung, D.R. Paul, Gas sorption and permeation in PIM-1, J. Membr. Sci. 432 (2013) 50–57.
[43] W.F. Yong, T.S. Chung, Mechanically strong and flexible hydrolyzed polymers of intrinsic microporosity (PIM-1) membranes, J. Polym. Sci. Part B: Polym. Phys. 55 (2017) 344–354.
[44] K.Y. Wang, Y. Xiao, T.S. Chung, Chemically modified polybenzimidazole nanofiltration membrane for the separation of electrolytes and cephalexin, Chem. Eng. Sci. 61 (2006) 5807–5817.
[45] T. Sugama, Hydrothermal degradation of polybenzimidazole coating, Mater. Lett. 58 (2004) 1307–1312.
[46] M.-Y. Hua, H.-C. Chen, R.-Y. Tsai, S.-J. Tseng, S.-C. Hu, C.-D. Chiang, P.-J. Chang, Preparation of polybenzimidazole-carboxylated multiwalled carbon nanotube composite for intrinsic sensing of hydrogen peroxide, J. Phys. Chem. C 115 (2011) 15182–15190.
[47] W.H. Lin, R.H. Vora, T.S. Chung, Gas transport properties of 6FDA-durene/1, 4-phenylenediamine (pPDA) copolyimides, J. Polym. Sci. Part B: Polym. Phys. 38 (2000) 2703–2713.
[48] W. Yong, F. Li, Y. Xiao, P. Li, K. Pramoda, Y. Tong, T.S. Chung, Molecular engineering of PIM-1/Matrimid blend membranes for gas separation, J. Membr. Sci. 407 (2012) 47–57.
[49] Z.P. Smith, R.R. Tiwari, T.M. Murphy, D.F. Sanders, K.L. Gleason, D.R. Paul, B.D. Freeman, Hydrogen sorption in polymers for membrane applications, Polymer 54 (2013) 3026–3037.
[50] A. Torrisi, C. Mellot-Draznieks, R.G. Bell, Impact of ligands on CO2 adsorption in metal-organic frameworks: first principles study of the interaction of CO2 with functionalized benzenes. II. Effect of polar and acidic substituents, J. Chem. Phys. 132 (2010) 044705.
[51] T. Yang, T.S. Chung, High performance ZIF-8/PBI nano-composite membranes for high temperature hydrogen separation consisting of carbon monoxide and water vapor, Int. J. Hydrog. Energy 38 (2013) 229–239.